Eur. Phys. J. Plus (2023) 138:946
https://doi.org/10.1140/epjp/s13360-023-04602-0

THE EUROPEAN PHYSICAL JOURNAL PLUS

Regular Article

The effects of the variable mass on the electronic and nonlinear optical properties of octic anharmonic oscillators

S. Sakiroglu[1,a], **M. B. Yücel**[2], **E. Kasapoglu**[3]

[1] Physics Department, Faculty of Science, Dokuz Eylül University, 35390 Izmir, Turkey
[2] Physics Department, Faculty of Science, Akdeniz University, 07058 Antalya, Turkey
[3] Physics Department, Faculty of Science, Sivas Cumhuriyet University, 58140 Sivas, Turkey

Received: 19 July 2023 / Accepted: 14 October 2023
© The Author(s), under exclusive licence to Società Italiana di Fisica and Springer-Verlag GmbH Germany, part of Springer Nature 2023

Abstract In this paper, we investigate theoretically the effects of a spatially varying effective mass distribution on the electronic and optical properties of octic anharmonic oscillators. Calculations to determine eigenvalues and eigenfunctions of the electron are performed within the effective mass approximation by using the diagonalization method. Optical absorption coefficients are obtained from the two-level approach in the density matrix expansion. Numerical results show that the position-dependent effective mass has a significant effect on the electronic energies and transitions between the subbands in single and double octic anharmonic oscillators. Furthermore, it was found that the optical properties of the system can be tailored in accordance with the desired purpose by changing the structural parameters of the system determining the size and the shape and with a proper choice of effective mass distribution.

1 Introduction

The quantum harmonic oscillator (HO) is a fundamental model in quantum mechanics that describes the behavior of a particle in a potential that is quadratic in its displacement from equilibrium. An anharmonic oscillator (AHO) potential is defined with the potential function that deviates from the harmonicity and these potentials have applications in various areas of physics, including molecular and solid-state physics. The eigenvalues and eigenstates of an AHO potential can be obtained using both analytical and numerical methods. Analytical methods involve solving the Schrödinger equation for the anharmonic potential by making approximations or using perturbation theory. Numerical methods involve using algorithms to solve the Schrodinger equation numerically.

Overall, AHO potentials are of great interest to scientific researches due to their important role in the evolution of many branches of quantum physics. Both numerical [1–9] and analytical techniques [10–13] have been used to study these potentials, and they have found applications in a wide range of fields, including molecular and solid-state physics. As is known, anharmonic oscillators are often encountered in molecular vibrations where the potential energy function is not entirely quadratic but contains higher-order terms that describe deviations from ideal harmonic behavior. Diatomic molecules are oscillatory systems in which nuclei vibrate around their equilibrium positions, and the vibrational motion of these systems is often modeled using the harmonic and anharmonic oscillator potentials, depending on the accuracy of the model. In this context, when studying the vibrational motion of diatomic molecules in quantum mechanics, the potential energy function describing the interaction between two atoms must include higher-order terms such as sextic, octic, and decatic. Non-harmonic effects become important at high vibration energy levels, where deviations from the harmonic approximation become more pronounced. Furthermore, AHO potentials with higher-order anharmonic terms have been extensively studied because they play an essential role in quantum tunneling time problems and molecular spectra [14–22]. The restrictions on the movement of particles confined within the low-dimensional semiconductor materials which have different size and shape very clearly affect the linear and nonlinear optical properties of materials such as absorption, refractive index changes, second- and third-harmonic generations of the semiconductor heterostructures, and these properties are of great importance in the productions and applications of optoelectronic devices such as high-speed electro-optical modulators, optical switching, infrared photo-detectors, semiconductor lasers, and far-infrared laser amplifiers [23–30]. By changing the structure parameters of low-dimensional semiconductor materials such as shape, size, width, and depth, as well as applying external fields such as electric, magnetic, and intense laser fields, the electronic, linear, and nonlinear optical properties of these materials can be appropriately tuned. Therefore, since the nonlinear optical effects of low-dimensional semiconductor materials are a hot topic for both theoretical and experimental research, the linear and nonlinear optical properties of these materials have been and will continue to be intensively studied [31–35].The octic AHO is a theoretical model used in quantum mechanics to study the behavior

[a] e-mail: serpil.sakiroglu@deu.edu.tr (corresponding author)

Published online: 24 October 2023

of particles in a potential that has an eighth-order anharmonic term. The systems with position-dependent effective mass (PDM) or variable mass are the focus of interest for researchers because of their importance in many branches of physics, especially in the study of the electronic and optical properties of semiconductors [36–45]. For instance, Herling and Rustagi studied the PDM effect on the optical properties of finite parabolic quantum well [37]. Magnetic field-related changes in the binding energy of a hydrogenic donor impurity in quantum wells defined by square and V-shaped potentials considering PDM approach are reported in Ref. [38]. The solution of the effective mass Schrödinger equation for the Morse potential is presented by Ovando and coworkers [40]. The influence of PDM on the binding energy of hydrogenic impurities in quantum dots with different confinement potentials has been reported in Ref. [42, 43]. Although several works were done on the electronic and optical properties of semiconductors with PDM, the influence of the spatially varying mass on the energy levels and intersubband optical absorption in a quantum well system defined with an octic anharmonic oscillator model profile has not been studied so far. This situation forms the basis of motivation for our study.

2 Theory

In the effective mass approximation, Hamiltonian for the electron is given by

$$H = -\frac{\hbar^2}{2}\left(\vec{\nabla}\frac{1}{m(z)}\vec{\nabla}\right) + V(z) \tag{1}$$

$m(z)$ is the mass of the electron that takes into account the fact that the effective mass of a particle can vary symmetrically as a function of position. Besides its convenient analytical nature, its shape is the familiar ineffective model of condensed matter and low-energy nuclear physics and depicts a soft symmetric distribution. $m(z)$ is defined below [46, 47]:

$$m(z) = m^* \mathrm{sech}^2\left(\frac{\pi z}{d}\right) \tag{2}$$

where d-parameter describes the effective length of position-dependent effective mass distribution, $m^* = 0.067m_0$ is the effective mass at $z = 0$, and m_0 is the free electron mass. It should be noted that, in this study, GaAs material parameters were used and $m^* = 0.067m_0$ is the effective mass of the electron in the GaAs material. At sufficiently large d values, the variable mass approaches the value of electron mass in the bulk material of interest, and the uniform behavior, stability, and spatial extension of the effective mass also increase. Admittedly, the choice of the PDM is not unique, in accordance with the nature of the problem [48, 49] and the chosen potential. The fact that the spatial dependence of the effective mass fits very well with the probability density profile of a particle in the ground state is an important reason for choosing this PDM model. $V(z)$ is the confinement potential. In the standard octic oscillator model, the potential energy function is given by

$$V(z) = V_0(\lambda_1(z/k)^2 + \lambda_2(z/k)^8) \tag{3}$$

where V_0 is the depth of the quantum well, k-parameter is related to the well width, λ is the coupling parameter, and also related to the width of the well. Depending on the choice of the parameters λ_1 and λ_2, the confinement potential becomes single or double octic AHO potential.

The variable mass changes the behavior of the system in several ways. First, the eigenfunctions and eigenvalues of the Hamiltonian are affected. The position-dependent effective mass modifies the wave functions, which leads to the changes in the energy levels of the system. These changes affect the stability and behavior of the system. Second, in the case of the double octic AHO, variable mass can also affect the tunneling behavior of the system. Overall, the position-dependent mass is an important factor to consider when studying the electronic properties and band structure of semiconductors. It can lead to interesting and potentially useful effects in these materials.

In order to solve Eq. (1), we used the diagonalization method by choosing orthonormal base functions that are solutions of an infinite square quantum well with L-width. L is infinite well width at the far end of QW which is large enough when comparing with the quantum well width which is considered. The L-v value is determined according to the convergence of the energy eigenvalues. The bases are formed as [46]:

$$\varphi_n(z) = \sqrt{\frac{2}{L}}\cos\left(\frac{n\pi z}{\mathrm{L}} - \delta_n\right), \tag{4}$$

where δ_n is

$$\delta_n = \begin{cases} 0, & n\,is\,odd \\ \frac{\pi}{2}, & n\,is\,even \end{cases}, \tag{5}$$

and so, the wave function in the z-direction is expanded in a set of basis function as follows

$$\psi(z) = \sum_{n=1}^{N} c_n\varphi_n(z), \tag{6}$$

where N is the size of the matrix. When calculating the wave function $\psi(z)$, we ensured that the eigenvalues are independent of chosen infinite quantum well width-L, and the wave functions are localized in the well region. This method requires embedding any well potential into an infinite square well, whose presence of the confining walls has no effect on the solutions. The width of the infinite square well has been chosen large enough so that the solutions are not sensitive to infinite walls. Further, the size of the matrix (the upper limit-N of the sum in Eq. (6)) is increased until convergence to any desired accuracy is achieved. It should be noted that in this study, the value of N is chosen large enough to guarantee a precise accuracy also for all confined states in different types of quantum wells considered. Immediately after the energies and related wavefunctions are acquired, linear and nonlinear absorption coefficients are found for transitions between any two electronic states by using the perturbation expansion and the density matrix methods.

Using the relevant approaches mentioned before, expressions of the linear, third-order nonlinear and total absorption coefficients (ACs) for the optical transitions are found as follows [37, 50], respectively

$$\beta^{(1)}(\omega) = \omega\sqrt{\frac{\mu_0}{\varepsilon_r}}\frac{\left|M_{ji}\right|^2\sigma_v\hbar\Gamma_{ji}}{(E_{ji}-\hbar\omega)^2+(\hbar\Gamma_{ji})^2} \tag{7}$$

$$\beta^{(3)}(\omega, I) = -2\omega\sqrt{\frac{\mu_0}{\varepsilon_r}}\frac{I}{\varepsilon_0 n_r c}\frac{\left|M_{ji}\right|^4\sigma_v\hbar\Gamma_{ji}}{\left[\left(E_{ji}-\hbar\omega\right)^2+\left(\hbar\Gamma_{ji}\right)^2\right]^2}$$
$$\left(1-\frac{\left|M_{jj}-M_{ii}\right|^2}{\left|2M_{ji}\right|^2}\frac{\left(E_{ji}-\hbar\omega\right)^2-\left(\hbar\Gamma_{ji}\right)^2+2E_{ji}\left(E_{ji}-\hbar\omega\right)}{E_{ji}^2+\left(\hbar\Gamma_{ji}\right)^2}\right) \tag{8}$$

$$\beta(\omega, I) = \beta^{(1)}(\omega) + \beta^{(3)}(\omega, I) \tag{9}$$

where $\varepsilon_r = {n_r}^2\varepsilon_0$ is the real part of the permittivity, σ_v is the carrier density in the system, μ_0 is the vacuum permeability, $E_{ji} = E_j - E_i$ is the energy difference between two states, $M_{ji} = \left|\langle\psi_j|ez|\psi_i\rangle\right|$, $(i,\ j = 1,\ 2)$ is the transition matrix element between the eigenstates ψ_i and ψ_j for incident radiation polarized in the z-direction, $\Gamma_{ji} = 1/T_{ji}$ is the relaxation rate, T_{ji} is the relaxation time, c is the speed of the light in free space, and I is the intensity of incident photon with the ω -angular frequency that leads to the intersubband optical transitions.

3 Results and discussions

In this section, we present the numerical results for the effect of PDM on the energy levels and optical transitions in single and double octic AHO. The used parameter values in our numerical calculations are: $\varepsilon_r = 12.58$, $V_0 = 228$ meV, $n_r = 3.2$, $T_{21} = 0.2ps$, $\mu_0 = 4\pi \times 10^{-7}\mathrm{Hm}^{-1}$, $\sigma_v = 3.0 \times 10^{22}$ m^{-3}, and $I = 5.0 \times 10^8$ $\mathrm{W/m}^2$. These parameters are suitable for GaAs/GaAlAs heterostructures [14].

Figure 1a presents the variation of the first four energy levels of an HO potential with respect to the k-parameter by considering two different values of the d-parameter describing the effective length of spatially varying mass distribution. In order to find out the effect of PDM, we also give the results under the assumption of a constant effective mass. For $\lambda_1 = 0.5$, the system is single-quantum well-called harmonic oscillator and as seen from the figure all the energies are decreasing function of k-parameter where the decrease becomes smoother for the smaller value of the d-parameter under consideration. Increment in d-parameter tends the variation of the mass to extent over the spatial region that explains the almost overlap of energies for $d = 50$ nm and constant effective mass approximation (solid lines), especially for the two lowest energy levels. It should be noticed that the energies of all levels have greater values in case of $d = 10$ nm as expected. In order to assist the interpretation of the absorption coefficients of HO system, in Fig. 1b we present the variation of the energy differences as a function of width parameter-k considering the same parameters as in Fig. 1a. Energy interval between any two levels is a decreasing function with an increase in k value except E_{34} that changes its variation after approximately $k = 6.5$ nm for PDM with d-parameter of 10 nm. Besides, energy intervals show a very small difference for $d = 50$ nm in comparison with the constant mass approximation where an equal spacing of energy between any two considered states exists.

Effect of PDM approach on the total absorption coefficient for an electron confined in octic AHO potential defined by $\lambda_1 = 0.5$ as a function of photon energy for width parameter of 5.0 nm and $d = 10$ nm is demonstrated in Fig. 1c. As seen from the figure, total absorption peaks for all considered transitions between the first four energy levels appear at the same position in case the PDM effect is not taken into account because of the equal energy intervals between specified states. Considering the spatially varying effective mass results with a blue-shift in the resonance peak of the total absorption coefficients, compared to the constant mass case, in accordance with the observations seen in Fig. 1b. In addition, as a consequence of improved transition matrix elements amplitude of the resonant peak of the total absorption coefficient enhances for PDM approach contrarily to the constant mass approximation where all three resonant peaks associated with the first three intersubband transitions overlap.

Variation from single parabolic-like potential profile to a strongly confined single quantum well structure with nearly hard-wall form can be obtained by choosing the coupling parameters $\lambda_1 = \lambda_2 = 0.5$. In Fig. 2a, we demonstrate the dependence of the first four

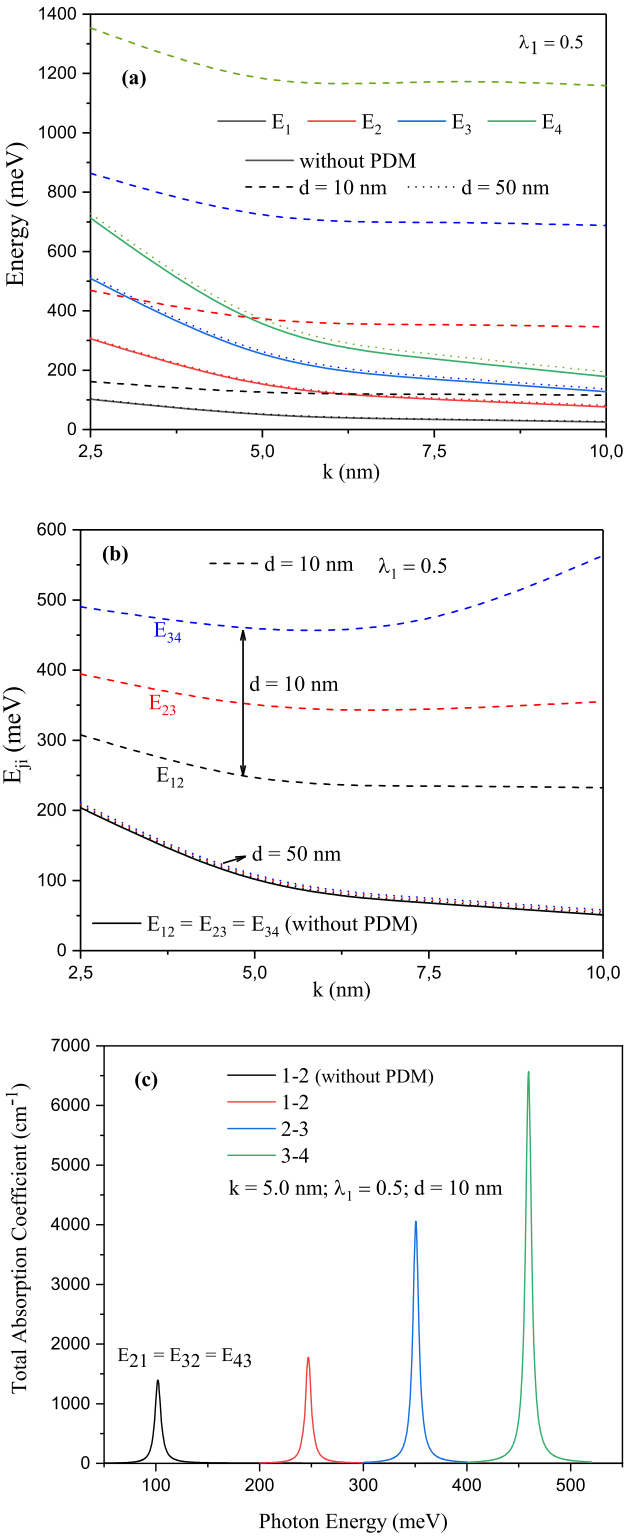


Fig. 1 **a** Variation of the first four energy levels of the HO with respect to k-parameter by considering two values of d-parameter ($d = 10$ nm and $d = 50$ nm). Solid lines represent the case for a constant mass approximation. **b** Energy differences between specified energy levels versus k-parameter for the same parameter set shown in (**a**). **c** Total optical absorption coefficients as a function of photon energy for the width parameter-k of 5 nm and PDM defined with $d = 10$ nm. In all subfigures, we use $\lambda_1 = 0.5$

energy levels of single octic AHO potential on the width parameter-k by considering constant effective mass case and two different values of the d-parameter associated with the varying mass distribution. Solid lines represent the constant mass approximation while dashed (dotted) lines stand for the case of varying mass distribution defined by $d = 10$ nm ($d = 50$ nm). It is seen that all the energies of single octic AHO are decreasing function of the k-parameter as a consequence of the widening of the well width. However, in comparison with the HO potential case, magnitudes of energies are enhanced and are not equally spaced because of the strengthening in confinement of the well potential. Another striking feature of this figure is the very smooth variation in energy at higher values

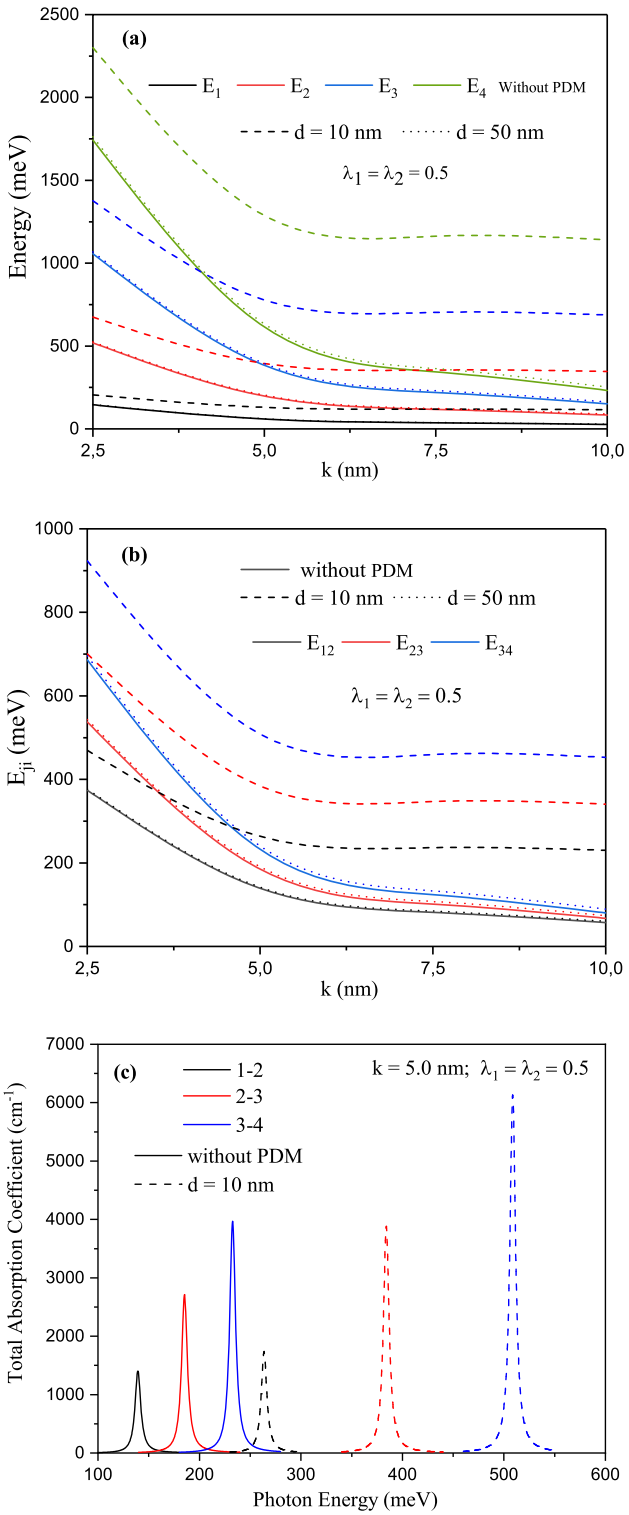


Fig. 2 **a** Variation of the first four energy levels of single octic AHO with respect to k-parameter for two different d-parameter values associated with PDM. Solid lines show the case for constant mass approximation. **b** Energy difference between two indicated electronic states versus k-parameter considering the same parameter set given in (**a**). **c** The variation of the total optical absorption coefficient as a function of incident photon energy for k-parameter of 5.0 nm and PDM with $d = 10$ nm. In all subfigures, we use coupling parameters $\lambda_1 = \lambda_2 = 0.5$

of the k-parameter as a result of weakened potential. Figure 2b demonstrates more clearly the dependence of the energy differences between the four lowest states as a function of the k-parameter considering the same parameter set as in Fig. 2a. Increment in k-parameter causes weakening of confinement potential that ends up with a decreasing behavior of the energy differences between considered energy levels. Total optical absorption coefficient of single octic AHO potential as a function of incident photon energy is shown in Fig. 2c for k-parameter of 5.0 nm where solid (dashed) lines correspond to the case without PDM (with PDM of $d = 10$ nm). Taking into account the spatially varying mass approximation brings about the blue-shift in position of resonant peak with a significant enhancement in the peak amplitude specifically for transitions between the higher states. Comparison with the single

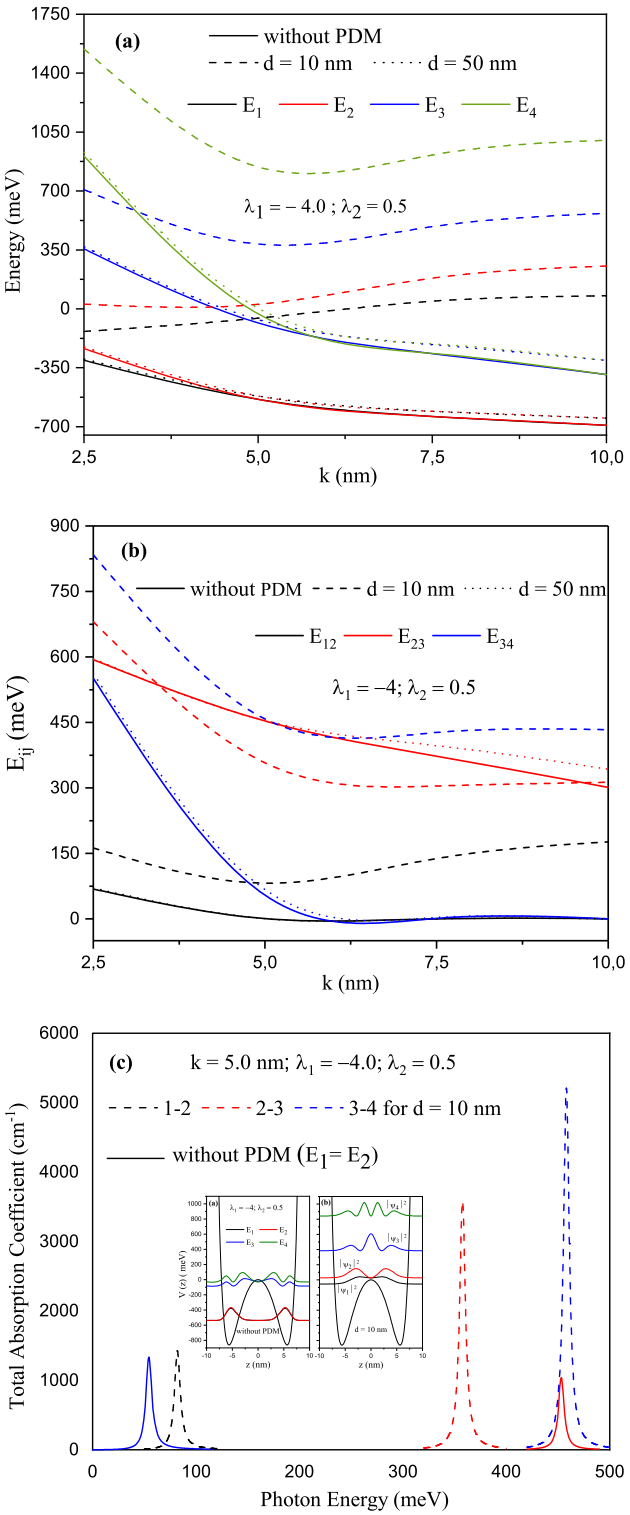


Fig. 3 **a** Variation of the first four energy levels of a double octic AHO versus the k-parameter for parameters $d = 10$ nm and $d = 50$ nm describing the spatially varying effective mass. **b** Energy difference between two electronic states under consideration as a function of k-parameter taking into account the same parameter set used in (**a**). **c** Total optical absorption coefficient as a function of incident photon energy for width parameter-k of 5 nm and PDM defined by $d = 10$ nm. In all subfigures, we use $\lambda_1 = -4.0$ and $\lambda_2 = 0.5$. Insets in **c** show the double octic AHO confinement profile, and squared wave functions corresponding to the first four energy levels in the cases of without and with PDM, respectively

well defined by $\lambda_1 = 0.5$ reveals the further shift toward higher energies in the position of the resonant peak due to the increased energy difference between states as a result of the sharpening of the well walls and its strengthening.

By an appropriate tuning of the coupling parameters, the system can be converted from a single octic AHO to a double octic AHO well form. For this purpose, in Fig. 3a the variation of first four energy levels as a function of the k-parameter is presented for coupling parameters $\lambda_1 = -4.0$ and $\lambda_2 = 0.5$. Influence of PDM approximation is given for two different values of the d-parameter. Solid lines represent the constant mass approximation, while dashed (dotted) ones represent the case of variable mass defined by $d = 10$ nm ($d = 50$ nm). We see that all the energies are decreasing functions of k-parameter in cases of without PDM and with PDM

defined by $d = 50$ nm. Moreover, an increment in the width parameter-k results with a degeneracy between considered energy states because of the combined effect of weakening in the confinement of double octic AHO potential and decoupling of two single wells. For the higher levels, the degeneracy occurs at larger k values. For varying mass distribution defined with $d = 10$ nm, the first two lowest state energies are smoothly increasing while the other two higher state energies show decreasing k-dependent behavior in the strong regime. Dependence of the energies to the confinement regime adjusted by the width parameter-k becomes less sensitive in weak confinement regime. In Fig. 3b, energy differences between specified energy levels as a function of the k-parameter considering the same parameter set as in Fig. 3a are given. Enhancement in k-parameter ends up with a decrease in the energy difference. For $d = 10$ nm, all the three energy spacing are smoothly varying function with k-parameter, whereas for $d = 50$ nm, k-dependence of E_{12} is almost the same as without PDM case, while E_{34} (E_{23}) show a sharp (almost linear) decrement with k-parameter. The reflection of these behaviors on the total optical absorption coefficient is seen in Fig. 3c where we take into account a system defined by width parameter-$k = 5.0$ nm and consider cases with constant mass approximation and PDM of $d = 10$ nm. In comparison with constant mass approximation results, resonant peaks corresponding to transitions between the second-third and the third-fourth states appear at lower and higher energy regions of the photon energy scale, respectively. In order to better explain the results here, double octic AHO potential profiles and the first four square wave functions corresponding to the relevant energies in the absence and presence of PDM are given as insets in Fig. 3c, respectively. As seen in the inset (a), the 1st and 2nd energy levels are twofold degenerated since the barrier width is wide to have no coupling between the wells. The 3rd and 4th electronic levels are above the potential barrier and are not degenerate anyway. Therefore, the total absorption peaks corresponding to the (1–2) transition cannot be observed while the (2–3) and (3–4) transitions are observed. In inset (b), with the effect of PDM, degeneracy disappears as the electronic energies shift toward higher energies and total absorption peaks belonging to the transitions between all levels considered are observed. Another important outcome of obtained total absorption coefficient results for single and double octic AHO well is the red-shift of the resonant peak position for a quantum well with coupling parameters $\lambda_1 = -4.0$ and $\lambda_2 = 0.5$ because of the weakening of confinement potential. It is seen that the competition between position dependency of mass and the width parameter-k determined the electronic and optical response of the system. Obtained numerical results exhibit that the optical response of octic AHO well can be tailored by a proper choice of the structural parameters, especially for sufficiently small d values.

4 Conclusion

In this paper, we have studied the intersubband optical transitions in a single and double octic AHO quantum well considering the influence of position-dependent effective mass. Energy levels are obtained by solving the effective mass equation through the diagonalization method approach. Numerical results reveal that the spatially varying effective mass has a significant effect on energy levels and optical response of the system. Energy states and difference between them decrease with increase in k-parameter that is related with the well width. Especially in double octic AHO system, nonuniformity of the effective mass through quantum system ends up with complicated behavior of energy variations that determines the optical outcome of the system. In double quantum wells, the tunneling effect can be enhanced by engineering the structure of the wells and barriers to create regions where the particles have a high probability of tunneling. This can be used to create devices such as resonant tunneling diodes and quantum cascade lasers, which rely on the controlled tunneling of electrons to function.

Author contribution SS was involved in writing, formal analysis, investigation; MBY helped in methodology, formal analysis, investigation; EK contributed to methodology, formal analysis, software, investigation, writing.

Data availability No new data were created or analyzed in this study. Data sharing is not applicable to this article.

Declarations

Competing interests The authors declare that they have no known competing financial interests or personal relationships that could have appeared to influence the work reported in this paper.

References

1. F. Maiz, M.M. Alqahtani, N. Al Sdran, I. Ghnaim, Phys. B: Cond. Matt. **530**, 101–105 (2018)
2. A.O. Adelakun, A.D. Dele, Adv. Phys. Theor. Appl. **27**, 38–43 (2014)
3. P. Gaudreau, R.M. Slevinsky, H. Safouhi, Ann. Phys. **337**, 261–277 (2013)
4. B.P. Shah, Int. J. Adv. Appl. Math. Mech. J. **2**, 102–109 (2014)
5. R. Budaca, P. Buganu, M. Chabab, A. Lahbas, M. Oulne, Ann. Phys. **375**, 65–90 (2016)
6. H. Ciftci, R.L. Hall, N. Saad, J. Phys. A.: Math. Gen. **38**, 1147–1155 (2005)

7. F. Maiz, M.M. Alqahtani, I. Ghnaim, AIP Con. Proc. **1976**, 020034 (2018)
8. P.J. Gaudreau, R.M. Slevinsky, H. Safouhi, Ann. Phys. **360**, 520–538 (2015)
9. F. Maiz, S. AlFaify, Phys. B Cond. Matt. **441**, 17–20 (2014)
10. A.J. Sous, J. Appl. Math. Phys. **3**, 1406–1411 (2015)
11. A.J. Sous, Mod. Phys. Lett. A **21**, 1675–1682 (2006)
12. A. de Souza Dutra, A.S. de Castro, H. Boschi-Filho, Phys. Rev. A **51**, 3480–3484 (1995)
13. G.M. Cicuta, S. Stramaglia, A.G. Ushvericze, Mod. Phys. Lett. A **11**, 119–129 (1996)
14. M.B. Yücel, E. Kasapoglu, C.A. Duque, Nanomaterials **12**, 1620 (2022)
15. F.M. Fernandez, R. Guardiola, J. Phys. A: Math. Gen. **26**, 7169 (1993)
16. I.A. Ivanov, J. Phys. A: Math. Gen. **31**, 5697 (1998)
17. M. Jafarpour, D. Afshar, J. Phys. A: Math. Gen. **35**, 87 (2002)
18. L.K. Sharma, J.O. Fiase, Eur. J. Phys. **21**, 167 (2000)
19. A.D. Speliotopoulos, J. Phys. A: Math. Gen. **33**, 3809 (2000)
20. A. Pathak, J. Phys. A: Math. Gen. **33**, 5607 (2000)
21. S.M. Ikhdair, R. Sever, Int. J. Mod. Phys. C **18**, 1571–1581 (2007)
22. T. Barakat, Phys. Lett. A **344**, 411–417 (2005)
23. N.D. Hien, Micro Nanostruct. **170**, 207372 (2022)
24. N.D. Hien, Physica E **145**, 115504 (2023)
25. N.D. Hien, Eur. Phys. J. B. **95**, 192 (2022)
26. J. You, K. Guo, J. Lao, S. Mo, Thin Solid Films **733**, 138813 (2021)
27. L. Zhang, H.-J. Xie, Phys. Rev. B **68**, 235315 (2003)
28. G. Wang, Phys. Rev. B **72**, 155329 (2005)
29. L. Zhang, J.-J. Shi, Phys. Stat. Sol. B **242**, 1001 (2005)
30. H. Yıldırım, M. Tomak, Phys. Rev. B **72**, 115340 (2005)
31. C.A. Duque, E. Kasapoglu, S. Sakiroglu, H. Sari, I. Sokmen, Appl. Surf. Sci. **257**, 2313–2319 (2011)
32. İ Karabulut, M.E. Mora-Ramos, C.A. Duque, J. Lumin. **131**, 1502–1509 (2011)
33. M.J. Karimi, G. Rezaei, J. Appl. Phys. **111**, 064313 (2012)
34. Z.-H. Zhang, K.-X. Guo, J.-H. Yuan, Physica E **108**, 238–243 (2019)
35. H.V. Phuc, N.D.A. Tuan, L. Dinh, Superlatt. Microstr. **100**, 1112–1119 (2016)
36. H. Sari, E. Kasapoglu, S. Sakiroglu, I. Sokmen, Optik **178**, 1280–1284 (2019)
37. G.H. Herling, M.L. Rustgi, J. Appl. Phys. **71**, 796–799 (1992)
38. H. Panahi, S. Golshani, M. Doostdar, Physica B: Cond. Matt. **418**, 47–51 (2013)
39. A. Khlevniuk, V. Tymchyshyn, J. Math. Phys. **59**, 082901 (2018)
40. G. Ovando, J.J. Peña, J. Morales, J. López-Bonilla, J. Phys. Conf. Ser. **792**, 012037 (2017)
41. A. John Peter, K. Navaneethakrishnan, Phys. Stat. Sol. B **220**, 897–907 (2000)
42. A. John Peter, K. Navaneethakrishnan, Physica E **40**, 2747–2751 (2008)
43. A. John Peter, Int. J. Mod. Phys. B **23**, 5109–5118 (2009)
44. R.M. Lima, H.R. Christiansen, Physica E **150**, 115688 (2023)
45. I. Maouhoubi, R. En-nadir, S. Maouhoubi, I. Zorkani, A.O.T. Hassani, A. Jorio, Physica E **148**, 115630 (2023)
46. H. Dakhlaoui, W. Belhadj, E. Kasapoglu, F. Ungan, Physica E **151**, 115737 (2023)
47. H.R. Christiansen, M.S. Cunha, J. Math. Phys. **55**, 092102 (2014)
48. A. Schulze-Halberg, J. Wang, J. Math. Phys. **56**, 072106 (2015)
49. S. Karthiga, V. Chithiika Ruby, M. Senthilvelan, M. Lakshmanan, J. Math. Phys. **58**, 102110 (2017)
50. M.G. Barseghyan, C.A. Duque, E.C. Niculescu, A. Radu, Superlatt. Microstruct. **66**, 10–22 (2014)

Springer Nature or its licensor (e.g. a society or other partner) holds exclusive rights to this article under a publishing agreement with the author(s) or other rightsholder(s); author self-archiving of the accepted manuscript version of this article is solely governed by the terms of such publishing agreement and applicable law.